Thermionic Emission of Negative Ions of Molecules and Small Clusters as a Probe of Low-Energy Attachment

Bruno Concina, Christian Bordas

Thermionic Emission of Negative Ions of Molecules and Small Clusters as a Probe of Low-Energy Attachment

Bruno Concina and Christian Bordas*

Université de Lyon, Université Claude Bernard Lyon 1, CNRS, Institut Lumière Matière, F-69622 Villeurbanne, France

Abstract

We have been studying thermionic emission of negatively charged molecules and small clusters for more than a decade. Kinetic energy released distribution (KERD) of mass-selected negative ions have been measured in a velocity map imaging spectrometer. Comparison of the experimental KERD to detailed balance models provided information on the reverse process, namely the electron attachment to the parent. The electron attachment to neutral systems (reverse process of the electron emission from anions) is usually described in a simplified way as a single electron capture in the framework of the classical Langevin model. Our measurements show that this approach is insufficient and that, in addition to the capture step, an Intramolecular Vibrational Redistribution (IVR) step should be included. As far as multiply charged anions are concerned, the electron attachment to anions (reverse process of the electron emission from dianions) is strongly affected by the repulsive Coulomb barrier (RCB). Previous studies assumed a pure over-the-barrier process, which is in disagreement with our study. Indeed, electron emission is measured below the RCB revealing significant thermal tunneling. In the present review, we summarize these works on singly and doubly charged anions in an attempt to present a unified view of the involved processes. It is worth noting that the detailed measurements of KERDs in the very low kinetic energy region (typically around 0.1 eV) has been made possible thanks to electron imaging methods without which all this work could never have been done, with in addition time-resolution capabilities allowing disentangling direct and delayed electron emission.

* corresponding author: christian.bordas@univ-lyon1.fr

1. Introduction

By analogy with bulk matter, where it is a common phenomenon, thermionic emission is defined in finite-size systems as a relaxation process by delayed electron emission of vibrationally excited species (molecules or clusters).[1–3] This electron emission statistically occurs after a given delay relatively to the excitation process (e.g. formation in an ion source or excitation by a laser). This delay can vary from nanosecond to millisecond (or even longer) depending on the internal energy content and on specific properties of the molecule or cluster (number of vibrational modes, electron binding energy…). Thermionic emission in finite-size systems was first evidenced at the beginning of the 90s on the basis of time-of-flight (TOF) spectra: a tail was observed following mass peaks as a direct consequence of the delayed character of this electron emission.[4,5] These pioneering works dealt with neutral systems including small metal clusters[4] and fullerenes.[5] In the case of the fullerenes, the tail was first fitted by a sum of three to four exponentials,[6] latter it was shown that the delayed electron emission follows a power law in time, with an exponent providing information about the competition between delayed ionization and unimolecular fragmentation.[7] Nowadays, this kind of measurement has been much improved and is operated on molecular anions in a storage ring[8,9] or a cryogenic ion-beam trap[10] giving access to delay range up to $100\ ms$ (or higher). This kind of device also allows to measure the delayed electron emission of hotter anions (excited by laser) on the millisecond time range.[11,12] Improvement of the vacuum ($\sim 10^{-14}\ mbar$) now makes it possible to store ions for hours and extends accordingly the time range of measurement of the decay of molecular anions.[13,14]

The rate constant is not the only relevant quantity defining thermionic emission. Additional and qualitatively very instructive information is provided by the kinetic energy released distribution (KERD). The latter was first measured on small anionic tungsten clusters (excited by a UV laser) with a magnetic bottle photoelectron spectrometer.[15] Two distinct components were visible on the spectra: at relatively high energy, the direct electron emission and at low energy, the thermionic emission. Unfortunately, the magnetic bottle apparatus is not well suited to the measurement of low energy ($< 0.2\ eV$) electrons and this led to an erroneous fit of the thermionic component of the KERD.[15] Product imaging as introduced in the 80's by Chandler and Houston for photofragment ions[16] and extended by Helm et al. to photoelectrons[17] was further improved in velocity map imaging (VMI) by Eppink and Parker.[18] Such a spectrometer is well adapted to the measurement of low energy electrons as the detection efficiency remains constant as a function of electron kinetic energy. Our group conducted a VMI experiment on small anionic tungsten clusters excited by a laser, which led to a robust measurement of the low energy spectra.[19] The latter, nevertheless, could contain a contribution from direct emission in addition to the thermionic one. In order to unambiguously disentangle the two types of electron emission, it was then proposed to implement a nanosecond gating of the microchannel plates (MCP) detector.[20] Thus it became possible to record time-resolved KERD. In particular, with a delay of about 100 ns relative to the laser excitation, the recorded spectrum does not contain direct electron emission anymore.[21,22] Using this experimental approach over a decade, we have conducted a detailed study on thermionic emission of various negatively charged molecules and small clusters excited by laser including small anionic tungsten clusters (as prototype of metal clusters),[23] fullerene anions[24] and dianions.[25] This method has been recently extended to the measurement of the spontaneous delayed electron emission in the case of the sulfur hexafluoride anion.[26]

Thermionic emission of anions of molecules and small clusters is a statistical process[2] and is closely related to the reverse process, i.e. electron attachment to the neutral, through the detailed balance principle.[27] In particular, the KERD explicitly depends on the cross section of the reverse process. Therefore, measuring the KERD of the electrons emitted by excited anions brings information on the electron attachment. Consequently, thermionic emission may be considered as a probe of this process.

Although our indirect method relies on a certain amount of modeling to extract the attachment cross section from the thermionic emission spectrum, it has some advantages in comparison to standard electron attachment experiments. More particularly, in the low-energy ($< 0.3\ eV$) crossed beam experiments, the electron current dramatically decreases, which prevents the measurement of cross sections.[28,29] In this type of work the experimental resolution was in the range of 30 to 150 meV and the zero of the energy scale had to be recalibrated using a known resonance of a molecule at threshold. (e.g. SF_6).[28,29] In contrast to electron attachment methods, the VMI spectrometer is more suitable for threshold measurements because of its energy-independent efficiency and better resolution at low kinetic energy. In addition, the origin of the energy scale is accurately estimated and corresponds to the center of the experimental image. Nevertheless, it should be mentioned that in comparison to standard crossed beam experiments, the EXLPA (extended energy laser photoelectron attachment) method strongly improves the accuracy of the measurements and led to robust cross section, like for SF_6 and CCl_4.[30] But it has only been applied to a limited number of molecules so far.

Measuring KERD of thermionic emission of anionic systems opens access to the electron attachment to the neutral, but appropriate modeling is required to extract relevant information from experimental results. The formation of anions can be described as a two-step process. In a first step, electron capture is induced by the polarization potential of the neutral system. In a second step, the electron excess energy is transferred to the vibrational modes and results in the formation of a stable state of the anion. This latter step is designated as Intramolecular Vibrational Redistribution (IVR). At the most elementary level of approximation, the capture cross section can be estimated within the framework of the classical Langevin model.[23] The quantum description of the electron capture process in the polarization potential was developed in the 1950s by Vogt and Wannier.[31] The quantum cross section fluctuates around the classical value, except at low energies where it converges to a value twice the Langevin limit.[31] In the specific case of C_{60}, it has been shown that the difference between classical and quantum estimates of the capture cross section remains less than 5% for energies larger than 4 meV.[32] Note that in the quantum description, the capture cross section results from a summation over partial waves of all possible values of orbital angular momentum ℓ. As IVR is expected to depend on the orbital angular momentum, only the quantum approach of Vogt and Wannier allows integration of the IVR into the capture cross section in order to obtain a realistic attachment cross section.[24,26,33,34]

In addition to singly charged anions, we have also studied model systems of multiply charged anions (MCA): the fullerene dianions C_{84}^{2-} and C_{90}^{2-}.[25,35] MCAs have been the focus of a great deal of interest due to the particular shape of the long-range interaction exerted on the outer electron. While in other molecular systems (neutrals, cations or singly charged negative ions) the outer electron undergoes a purely attractive potential, MCAs exhibit a long-range repulsive Coulombic interaction. The sum of this long-range repulsive interaction and the short-range attractive interactions results in the creation of a repulsive Coulomb barrier (RCB). The presence of this repulsive barrier is at the origin of specific features of MCA photodetachment.[36–38] In the case of the dianions, the reverse process is the electron attachment to the singly charged anion, in which the characteristics of the RCB are crucial. Measured KERDs demonstrate that a significant fraction of the electron emission occurs via tunneling through the RCB.[25] In order to describe the attachment cross section in the case where tunneling is present, a relatively simple expression can be used as a first approach. It consists in weighting the hard sphere approximation by the tunneling probability when the kinetic energy of the electron is below the repulsive barrier.[25,35]

2. Experimental setup

The key device of our experimental setup is the time resolved VMI spectrometer, schematically presented in Fig. 1.[20,39] Our VMI spectrometer is based on the standard design introduced in[18] and is set perpendicularly to the ion drift tube. The whole spectrometer is surrounded by a μ-metal cylinder acting as a screen towards external magnetic fields. Four circular holes are arranged in the μ-metal cylinder allowing the laser and ion beams to cross at right angles in the center of the VMI interaction region. The intersection between ion and laser beams is located on the spectrometer axis halfway between the pair of electrodes E_0 and E_1. The photoelectrons are subsequently accelerated by the stationary nonuniform electric field produced by the three electrodes E_0, E_1, and E_2. All electrodes are 66 mm in diameter and 20 mm apart. Photoelectrons are extracted through inner holes of 20-mm diameter in the center of E_1 and E_2 electrodes. A 93 mm long field-free region separates the E_2 electrode from the position-sensitive detector (PSD). Our PSD is a commercial assembly (F2225-21P, Hamamatsu, Japan) of a pair of 2-inches microchannel plates (MCP) combined with a phosphor screen. Electron impacts, amplified and converted to photons in the MCP-phosphor assembly, are subsequently recorded by a charge coupled device (CCD) camera (Stingray F-146B, Allied Vision Technologies) then transferred to a PC and summed over 10^4-10^6 laser shots before processing.

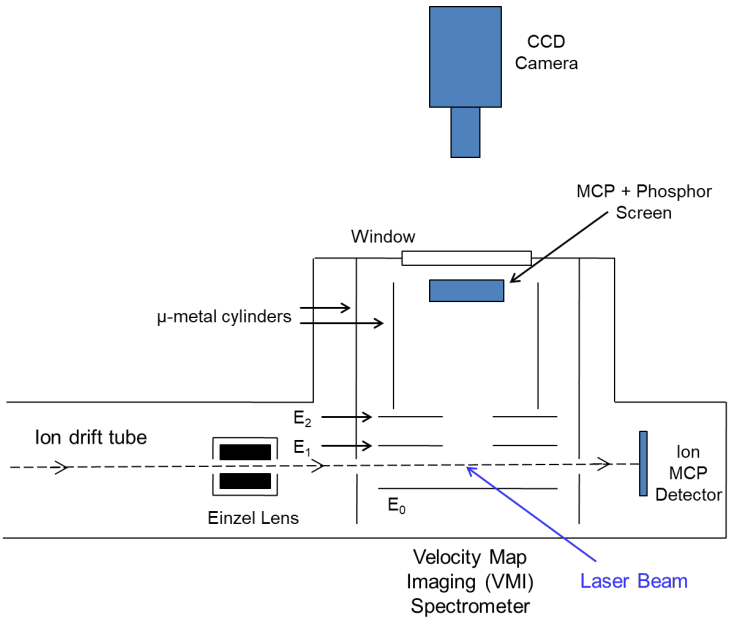

Figure 1: schematic layout of the time resolved velocity map imaging spectrometer.

Anions entering the spectrometer between electrodes E_0 and E_1 are deflected by the static electric field. Therefore, it is preferable to use sufficiently low field values in order not to deteriorate the overlap between the ion and laser beams. In addition, the voltages V_0 and V_1 applied to the electrodes E_0 and E_1 are adjusted as close as possible to the ground potential in order to avoid significant deformation of the ion bunch entering the interaction region. The voltage ratios allowing to achieve the proper operation of the VMI spectrometer are based on a first estimation obtained by numerical simulation and optimized on the images of atomic anions used for calibration (iodine[39] and fluorine[26] anions detached by a 349-nm pulsed laser[39]). In the present geometry the optimal ratio is found to be $(V_2 - V_1)/(V_2 - V_0) \approx 0.75$. Most experiments presented below were performed using the following

values: $V_0 = -130\ V$; $V_1 = 0\ V$; $V_2 = 400\ V$. These settings are even reduced by a factor of two for recording SF_6^- KERD which peaks at only 12 meV.[26]

Time resolution has been implemented in the VMI spectrometer in order to distinguish unambiguously between delayed and direct electron emission.[20,39] A resolution suitable for the processes under study is obtained by applying a high-voltage (HV) pulse to the detector. The input side of the pair of channel plates is set to the same constant voltage V_2 as the E_2 electrode. A HV pulse is applied between the input and output sides of the pair of channel plates at a 1-kHz repetition rate using a fast HV switch (HTS 31-03-GSM, Behlke, Germany) driven by a delay generator (DG 535, Stanford Research Systems, USA). The voltage difference between the two sides of the plates increases from 800 V to 1500 V during a softened square-shaped pulse of about 140 ns.[39] However, the gain of the detector is highly nonlinear as a function of the applied tension. As a result, the detection efficiency varies considerably for small changes in the applied tension. The detection efficiency for the base voltage (800 V) is thus totally negligible as compared to the efficiency for the maximum voltage during the pulse (1500 V). The gain curve of the detector is therefore significantly narrower than the HV signal, with a total width at half maximum (FWHM) of about 55 ns.[39] In early experiments performed on tungsten anions, a similar time-resolved detector was used but it was limited to a lower repetition rate (10 Hz).[23] The ability of separating direct from delayed emission is exemplified on Fig. 2 where the recorded spectra synchronized or delayed by 90 ns respectively are presented in the case of the anion W_{13}^-.

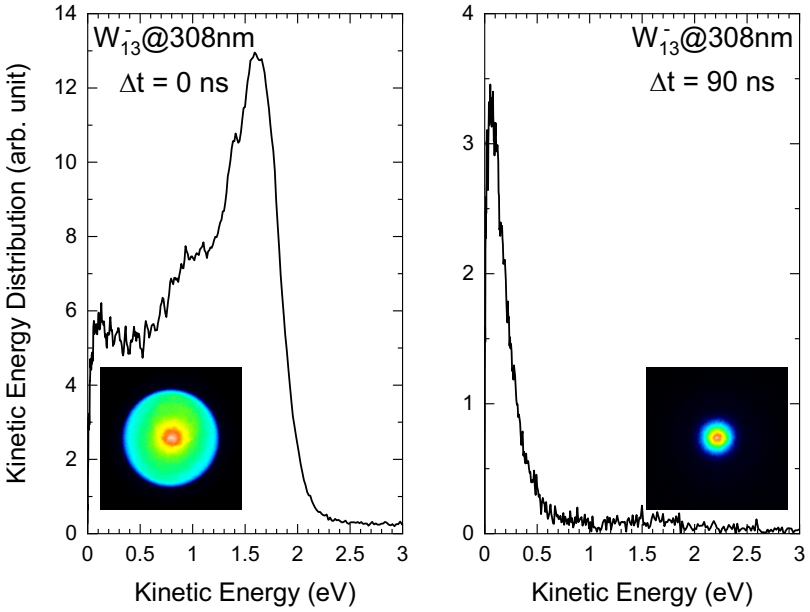

Figure 2: demonstration of capability to separate direct and delayed electron emission on W_{13}^- excited by laser. Kinetic energy distributions (inset: raw images) have been measured for two delays. On the left, the HV pulse peak is synchronized with the laser pulse. The distribution includes both direct and delayed electrons. On the right, the delay after the laser pulse has been increased to 90 ns and only pure delayed (thermionic) emission is detected without any contribution from direct detachment.

Different types of ion sources are used depending on the species of interest. They are briefly described below.

Tungsten clusters are produced in a laser vaporization source. A laser beam (532-nm wavelength pulsed at 10 Hz) is focused on a rotating tungsten rod.[23] This interaction produces a plasma that is cooled down by supersonic expansion in bunches of helium gas injected through a pulsed valve. The native anions are then perpendicularly extracted and accelerated by a pulsed electric field before entering the drift tube of a time-of-flight (TOF) mass spectrometer. Mass selected ion bunches enter the VMI spectrometer and adequate timing of the excitation laser (pulsed Xe:Cl laser ; wavelength of 308 nm) and of the high-voltage pulse applied to the PSD ensures excitation of a given cluster mass and measurement of the KERD.[23]

Fullerene anions and dianions are produced by electrospray ionization (ESI).[24,25,39] The ESI source is part of a commercial mass spectrometer, micrOTOF-Q (Bruker, Daltonics).[39] The selection of the ionic species of interest is achieved using a mass-selective quadrupole. At the output of the micrOTOF-Q, the ions are orthogonally accelerated into a linear TOF by a Wiley-McLaren assembly with HV pulsed at a 1-kHz repetition rate.[39] The linear TOF contains the VMI spectrometer mounted perpendicularly to the ion drift tube. The nanosecond pulsed detachment lasers operating at 1-kHz repetition rate are either a diode pumped Nd:YAG laser (1064 nm or 532 nm) or a diode pumped frequency tripled Nd:YLF laser (349 nm).

SF_6^- is produced in an Electron Cyclotron Resonance (ECR) ion source by electron attachment to the SF_6 gas.[26,40,41] A continuous beam of negative ions (and electrons) is extracted from the plasma by an acceleration voltage of a few kV and is mass analyzed by a 90° magnetic sector. The current of the continuous mass selected beam of SF_6^- is about 10 nA as measured by a Faraday cup. The continuous beam is pulsed using a parallel plate deflector, resulting in ion bunches of a few µs duration at 1-kHz rate. The ion bunches pass through a drift tube and enter the VMI spectrometer orthogonally mounted to the ion drift tube.

3. Detailed-balance formalism

Delayed electron emission from isolated molecules or clusters is described as a statistical process and is denoted as thermionic emission by analogy with bulk matter. Its general description relies on the hypothesis of a thermal equilibrium among all vibrational degrees of freedom. It is based on the detailed-balance principle, a consequence of microscopic reversibility.[2,35] The formalism introduced by Weisskopf for particle emission from nuclei[27] offers a suitable framework for application to statistical decay processes from molecules or small clusters,[3,42] like dissociation[43] or thermionic emission.[2] In the following, we restrict to the thermionic emission from a molecular anion or dianion, as exemplified by fullerene anions[24] or dianions:[25]

$$C_n^- \rightarrow C_n + e^- \quad \text{(1a)}$$
$$C_n^{2-} \rightarrow C_n^- + e^- \quad \text{(1b)}$$

We note with index i (initial) all quantities relative to the parent anion or dianion and with index f (final) all quantities relative to the daughter neutral or anion. The electron binding energy E_b is equal to the electron affinity EA of the neutral in the case of singly charged anions, or to the second electron affinity

EA_2 in the case of doubly charged anions. The differential rate for emission of an electron of kinetic energy ε from a parent of vibrational energy E reads[26]

$$k(E,\varepsilon) = \frac{m_e}{\pi^2\hbar^3}\frac{g_f}{g_i}\varepsilon\sigma(\varepsilon)\frac{\rho_f(E-E_b-\varepsilon)}{\rho_i(E)} \quad (2)$$

with m_e being the electron mass, g_i the electronic degeneracy of the parent, g_f is the product of the electronic degeneracy of the daughter by the spin degeneracy of the free electron. The vibrational density of states of the parent and daughter species are noted respectively ρ_i and ρ_f. In Eq. (2), it has already been assumed that the total density of states is equal to the product of the electronic degeneracy and of vibrational density of states. σ is the cross section of the reverse process, i.e., the electron attachment to the daughter. We introduce the daughter temperature T_d, defined as the microcanonical temperature of the daughter with vibrational energy $E - E_b$,[2,44]

$$\frac{1}{k_B T_d} = \frac{d}{dE}\ln\rho_d(E-E_b) \quad (3)$$

with k_B the Boltzmann constant and ρ_d the vibrational density of states of the daughter ($\rho_d = \rho_f$). $\ln\rho_f(E-E_b-\varepsilon)$ may be expanded through a Taylor expansion in powers of ε using the daughter temperature T_d.[26,35] The first order term leads to a Boltzmann factor. The expression of the second and third order terms depends on the heat capacity C_d (temperature derivative of the energy) of the daughter defined for $T = T_d$.[26] Finally, the differential rate may be written as[26]

$$k(E,\varepsilon) = \frac{m_e}{\pi^2\hbar^3}\frac{g_f}{g_i}\varepsilon\sigma(\varepsilon)\frac{\rho_f(E-E_b)}{\rho_i(E)}\exp\left(-\frac{\varepsilon}{k_B T_d} - \cdots\right) \quad (4)$$

with the dotted line denoting the second and third order terms (expressions available in ref. [26,35]). For both fullerene dianions and sulfur hexafluoride anion, it has been shown that an expansion up to the second order is required.[26,35] For the other systems (anionic tungsten clusters[23] and fullerene anions[24]), only the first term is used, which is the usual approximation.[2,45]

If it is reasonable to assume that parent and daughter have the same density of states of vibration ($\rho_f \approx \rho_i$), the logarithm of the common level densities $\rho(E-E_b)$ and $\rho(E)$ is developed around the median value $E - E_b/2$ leading to an expression containing only odd terms.[2,45] This step requires the introduction of the emission temperature defined as $T_e = T(E - E_b/2)$. The usual approximation consists in keeping only the first term, leading to an Arrhenius expression.[2,45] This point has been justified for fullerene dianions.[35] Finally, in the case where the vibrational densities of state of the parent and the daughter can be assumed identical, the differential rate for electron emission reads[35]

$$k(E,\varepsilon) = \frac{m_e}{\pi^2\hbar^3}\frac{g_f}{g_i}\varepsilon\sigma(\varepsilon)\exp\left(-\frac{E_b}{k_B T_e}\right)\exp\left(-\frac{\varepsilon}{k_B T_d} - \cdots\right) \quad (5)$$

By contrast, in the case of SF_6^-, the level densities of the anion and of the neutral differ so much (due to the change of geometry)[46] that the level densities are kept in place and are explicitly calculated (in the harmonic approximation) by the Whitten-Rabinovitch expression[26,47] as a function of the internal energy.

A caloric curve, i.e., the vibrational energy as a function of temperature, or at least the heat capacity, is required. For anionic tungsten clusters, due to the lack of information on these quantities, we use the classical harmonic expression for the microcanonical heat capacity: $C = (3n-7)k_B$.[23] This expression differs from the canonical heat capacity by $-k_B$.[2,44] The caloric curve of C_{60} is taken from

literature,[8] approximated by a linear expression and is scaled accordingly to the size for larger fullerene anions and dianions.[35] An analytical expression is derived for the caloric curve from the Whitten-Rabinovitch expression of level density and has been used for SF_6^-.[26]

Finally, the KERD reads in this theoretical approach,

$$f(\varepsilon) \propto \varepsilon\sigma(\varepsilon)\exp\left(-\frac{\varepsilon}{k_B T_d} - \cdots\right) \tag{6}$$

A critical ingredient of this formulation is the cross section $\sigma(\varepsilon)$ of the reverse process. In the next paragraphs, we will present the models used to describe the electron attachment to neutral and to anionic systems.

In our experiments, the KERD measurements occurs at a given delay t after the last energy exchange of the ion with the external medium (i.e., formation in an ion source or excitation by laser). This delay is about 40 µs for SF_6^- (spontaneous decay) and about 100 ns for the other systems (photoinduced decay). Qualitatively, the hotter molecular ions decay first. Quantitatively, the internal energy distribution of the ions decaying at a given time t is relatively narrow and peaks at the energy $\bar{E}$ given by

$$K(\bar{E}) = \frac{1}{t} \tag{7}$$

where $K(\bar{E})$ is the rate for electron emission from an ion of internal energy $\bar{E}$.[26,35] It is obtained by integration of the differential rate $k(E, \varepsilon)$ (as given by Eq. (4) or (5)) over kinetic energy ε . This relation allows the estimation of the daughter temperature T_d which can be compared to the experimental KERD or used as a benchmark.[23–26] This relation assumes that the electron emission is the only decay channel. Indeed, dissociation energies are much larger than the electron binding energy for these negatively charged systems.[23,48] Besides, the delays are short enough that radiative cooling may be disregarded.[10,49]

4. Thermionic emission from anions: beyond Langevin model for the description of electron attachment

As underlined above, the KERD depends on the cross section of the reverse process. In the case of the thermionic emission from anions, the latter is the electron attachment to the neutral. The classical Langevin model leads to an expression of the attachment cross section at the most elementary level of approximation:[23] it describes only the capture step via a simple $-c_4/r^4$ potential where $c_4 = \alpha\,(e/4\pi\varepsilon_0)^2/2$, α being the polarizability of the neutral, and it disregards the IVR step. The capture cross section σ is then given by

$$\sigma(\varepsilon) = 2\pi\sqrt{\frac{c_4}{\varepsilon}} \tag{8}$$

In this classical frame, the KERD reads

$$f(\varepsilon) \propto \varepsilon^{1/2} exp\left(-\frac{\varepsilon}{k_B T_d}\right) \tag{9}$$

with T_d the so-called daughter temperature. KERD measurements have been carried out on fullerene anions C_n^- $(n = 60, 70, 78, 84, 90)$.[24] The measured KERD profile depends on the fullerene size. In particular, sharp peaks are observed for C_{60}^- and C_{70}^- which cannot be fitted by the Langevin distribution given by Eq. (9), which is illustrated by Fig. 3.

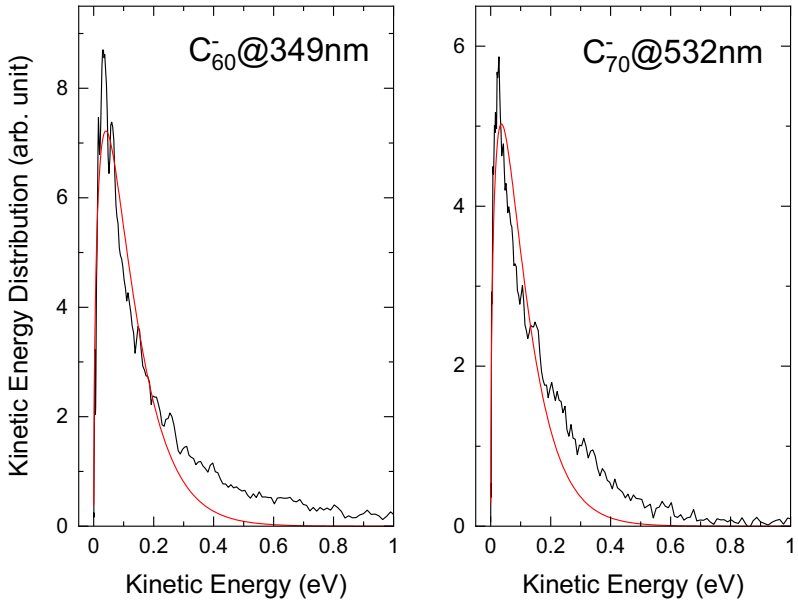

Figure 3: experimental kinetic energy distributions (black) of thermionic emission from the fullerene anions C_{60}^- and C_{70}^- excited by laser. They are compared to the fit (red) using the Langevin distribution (Eq. 9). The sharp experimental distribution cannot be fitted by the Langevin one.

This implies that one should use a more refined description of the electron attachment to the neutral fullerenes including IVR. As it is expected that the IVR depends on the orbital angular momentum ℓ, the classical Langevin model cannot be modified to include the IVR. It is necessary to use its quantum extension which was developed by Vogt and Wannier.[31] In this approach, the capture cross section σ is expressed as a sum over partial waves of angular momentum ℓ:

$$\sigma(k) = \sum_{\ell} \frac{\pi}{k^2}(2\ell + 1)P_\ell^{VW}(k) \tag{10}$$

where k is the wave vector and $P_\ell^{VW}(k)$ the capture probability for a given angular momentum ℓ. The angular dependence of the wave functions is given by the spherical harmonics. The $P_\ell^{VW}(k)$ are expressed as a function of the reduced wave vector $\kappa = k\sqrt{2m_e c_4/\hbar^2}$ which simply reads $\kappa = \sqrt{2\alpha\varepsilon}$ in atomic units.[24,50] Using the reduced wave vector, Eq. (10) becomes in atomic units,

$$\sigma(\kappa) = \sum_{\ell} \alpha\frac{\pi}{\kappa^2}(2\ell + 1)P_\ell^{VW}(\kappa) \tag{11}$$

Numerically accurate analytical fits for the $P_\ell^{VW}(\kappa)$ probabilities may be found in the literature.[51] The IVR is introduced through the empirical terms $P_\ell^{IVR}(\kappa)$ representing the probability that an electron capture results in a stable anion.

$$\sigma(\kappa) = \sum_{\ell} \alpha \frac{\pi}{\kappa^2}(2\ell+1)P_\ell^{VW}(\kappa)P_\ell^{IVR}(\kappa) \tag{12}$$

Empirical analytical expressions for $P_\ell^{IVR}(\kappa)$ have been proposed for the fullerene anions.[24] Finally, the κ-distribution used to fit the experimental ones reads[24]

$$f(\varepsilon) \propto \kappa exp\left(-\frac{\kappa^2}{2\alpha k_B T_d}\right)\sum_{\ell}(2\ell+1)P_\ell^{VW}(\kappa)P_\ell^{IVR}(\kappa) \tag{13}$$

with α in atomic units, T_d in Kelvin, and $k_B = 3.1668 \times 10^{-6} HK^{-1}$. Experimental κ distributions for the fullerenes C_{60}^- and C_{84}^- are presented in Fig. 4 with global fits and contributions of each partial wave. Information on the IVR has been deduced from the fit and has been interpreted using the molecular symmetries. The studied fullerenes exhibit very different symmetry properties depending on their size. It is well known that C_{60} belongs to the icosahedral point group I_h while C_{70} belongs to the D_{5h} point group. The larger fullerenes are observed in several isomeric forms of lower symmetry. For instance, two isomers D_2 and D_{2d} are observed for C_{84} in the ratio 2:1.[52] For these low symmetry molecules, the magnitudes of the P_ℓ^{IVR} factors tend to be independent of the orbital angular momentum ℓ. By contrast, C_{60} is characterized by a quite high magnitude for the IVR of *p*-symmetry (relatively to the d-symmetry) which can be associated to its high icosahedral symmetry. Indeed, in the I_h symmetry, the p waves transform as t_{1u} which is the symmetry of the LUMO.[24,53] Consequently, the symmetry of the electron wave function is similar when it is bound and when it is free, which may strengthen the electron phonon coupling. These results compare well with the literature. Our IVR estimate agrees with measurement of the thermal attachment rate to C_{60}, showing nice convergence between attachment and detachment studies.[24,34] Measurement of the electron attachment cross section to C_{60} at low energy reveals a deep minimum around 0.4 eV.[54] This feature can be related to the low magnitude of the d-wave in comparison to the p-wave (the d-wave reaches its maximum at 0.32 eV).

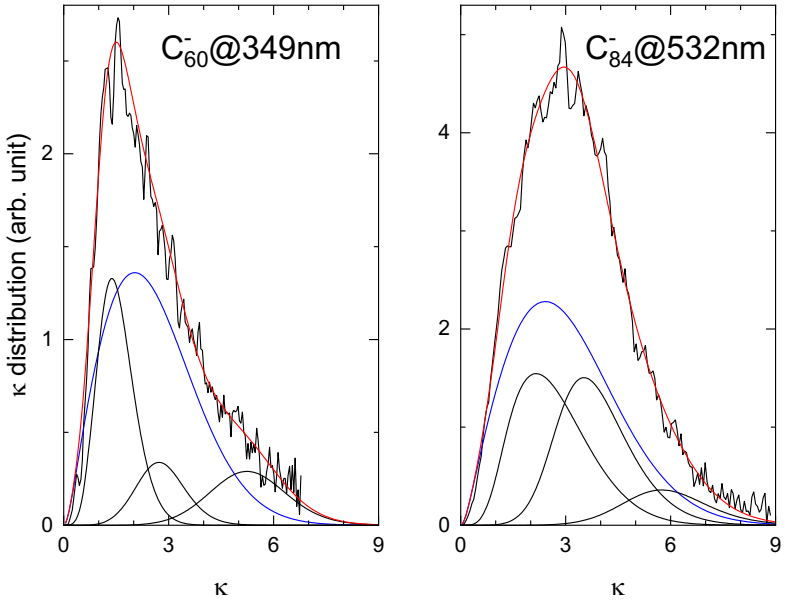

Figure 4: experimental κ distributions (black) of thermionic emission from the fullerene anions C_{60}^- and C_{84}^- excited by laser. They are compared to the global fit (red) resulting from the Vogt and Wannier theory including an IVR step. The relative contribution of the partial waves $\ell = 0,1,2,3$ is displayed (the s wave is plotted in blue, higher-order terms are plotted in black with increasing threshold when ℓ increases).

By contrast, in the specific case of SF_6^-, the Vogt-Wannier approach is much simpler as the attachment proceeds only by s-wave capture,[26,30]

$$\sigma(\kappa) = \alpha \frac{\pi}{\kappa^2} P_0^{VW}(\kappa) \tag{14}$$

After electron capture, two processes may occur: IVR, which stabilizes the anion, and vibrational excitation (VEX), which leads to electron release. More precisely, VEX is a direct collisional excitation of vibrations followed by electron release.[33] It has an energy threshold given by the quantum of the symmetric stretch mode A_{1g} (96.6 meV),[30] leading to a threshold in κ : $\kappa_0 = 0.560$. Finally, the non-dissociative electron attachment cross section reads

$$\sigma(\kappa) = \alpha \frac{\pi}{\kappa^2} P_0^{VW}(\kappa) P^{IVR}(\kappa) P^{VEX}(\kappa) \tag{15}$$

with $P^{IVR}(\kappa)$ the probability that IVR occurs and $P^{VEX}(\kappa)$ the probability that the vibrational excitation does not happen.[26] Empirical expressions are proposed and fitted to a high resolution measurement of the attachment cross section.[26,30] Consequently, there is little uncertainty on the attachment cross section, allowing a more stringent test of the thermionic emission modeling than in the case of the fullerene anions.

The experimental κ distribution for SF_6^- is reported in Fig. 5. It is compared to various fits including respectively different terms in the expression of the attachment cross section. The agreement with the experimental distribution is generally quite satisfactory, however the various fits lead to very different values of the daughter temperature T_d. Under the assumption of a pure s-wave capture, the daughter

temperature T_d is fitted to 479 K. This value is substantially larger than the value deduced in a simple Langevin model ($T_d = 319\,K$; not represented, see ref. [26]). Introducing a second step in the attachment process reduces the cross section even further and leads to an increase in the fitted value of the temperature: IVR alone leads to $T_d = 652\,K$, while IVR combined with VEX lead to $T_d = 667\,K$. Note the major influence of IVR while including VEX is of minor consequence on the fitted temperature because most of the κ distribution is defined below the VEX threshold ($\kappa_0 = 0.560$, indicated by a red arrow on Fig. 5).

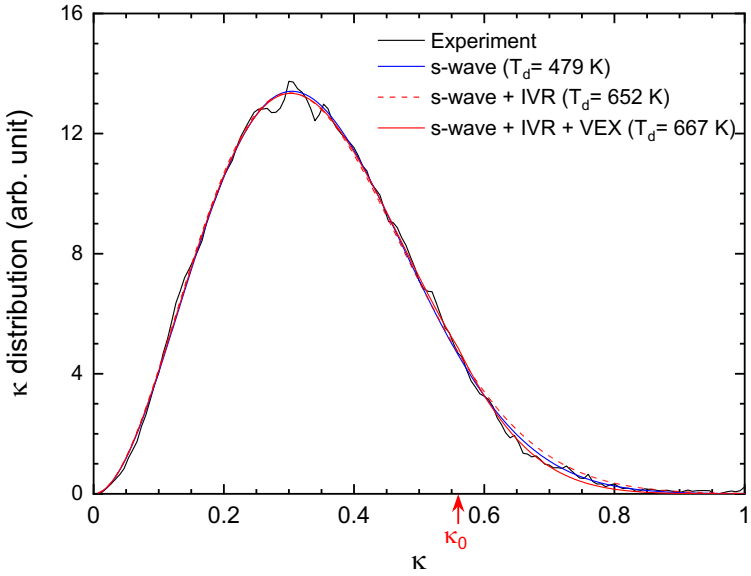

Figure 5: measured κ distribution (black line) of spontaneous thermionic emission from SF_6^-, compared to fits based on different assumptions regarding the attachment : pure s-wave capture (blue line), s-wave capture followed by IVR (dashed red line), and s-wave capture followed by IVR and VEX (full red line). VEX threshold ($\kappa_0 = 0.560$) is indicated by a red arrow.

Detailed balance should link truly reverse processes[26,33] between, on one hand, the anion in the electronic ground state and, on the other hand, the neutral and the electron infinitely separated. In our approach, the attachment consists of an electron capture followed by IVR. As VEX is in competition with IVR when the electron is captured, the probability $P^{VEX}(\kappa)$ should be included in the attachment cross section (see Eq. (15)). But the detachment is not concerned with VEX as the final state of VEX is not the initial state of the detachment (i.e., the anion in the electronic ground state). When comparing with experimental results, this point is not critical since most of the κ distribution is defined below the VEX threshold. Besides, above the VEX threshold, the fit of the attachment cross section allows only the determination of the product $P^{IVR}(\kappa)P^{VEX}(\kappa)$. Other expressions for both $P^{IVR}(\kappa)$ and $P^{VEX}(\kappa)$ might be assumed as long as the product remains the same. The remaining indeterminacy on the empirical terms prevents an exact derivation of the cross section used in the detailed-balance expression of the thermionic emission.

In the case of small anionic tungsten clusters W_n^- ($9 \leq n \leq 21$),[23] the shape of the experimental KERD was compared to the Langevin model using as a fitting function the generalized thermal distribution

$$f(\varepsilon) \propto \varepsilon^{\gamma} exp\left(-\frac{\varepsilon}{k_B T_d}\right) \quad (16)$$

where γ and T_d are both free parameters. In the framework of the Langevin model, the γ exponent is strictly equal to $1/2$. Estimation of the γ exponent from experimental KERD leads to values significantly lower than $1/2$, in the range 0.45-0.32, decreasing as the cluster enlarges.[23] When the γ exponent is set to the $1/2$ value, this fitting function leads to an estimate of the daughter temperature T_d in the framework of the Langevin model. This estimate may be compared with the daughter temperature T_d derived from Eq. (7) by writing the equality of the decay rate (as given by Eq. (5)) and of the inverse of the experimental delay.[23] Significant differences have been found between the two estimates in the size range 9-15 whereas a good agreement is noted for larger sizes up to 21. We have interpreted the disagreement between the two series of temperatures as due to a capture cross section lower than the classical Langevin cross section given by Eq. (8). We assume that the attachment cross section σ is equal to the product of a sticking probability s times the Langevin capture cross section. In this simple approach, the probability *s* does not depend on the kinetic energy ε. It is determined by writing that the inverse of the experimental delay is equal to the decay rate given by Eq. (5) where the attachment cross section σ is given by the factor *s* times the Langevin cross section and where the daughter temperature T_d is deduced from the experimental KERD. The sticking probability *s* is displayed in Fig. 6 as a function of cluster size. This coefficient is close to unity for large clusters, while it ranges between 10^{-2} and 10^{-1} for smaller systems in the size range *n*=9-14. The sticking probability, i.e., the reduction of the attachment cross section in comparison to the Langevin capture cross section, may be interpreted as being due to the IVR. Besides, the fact that the γ exponent is found lower than the Langevin value of $1/2$ may be qualitatively explained by a slight overrepresentation of the partial waves of low orbital angular momentum ℓ. These partial waves are favored by the IVR process: the probability of forming a stable anionic state is expected to be slightly higher for low values of the orbital angular momentum ℓ relatively to higher values.

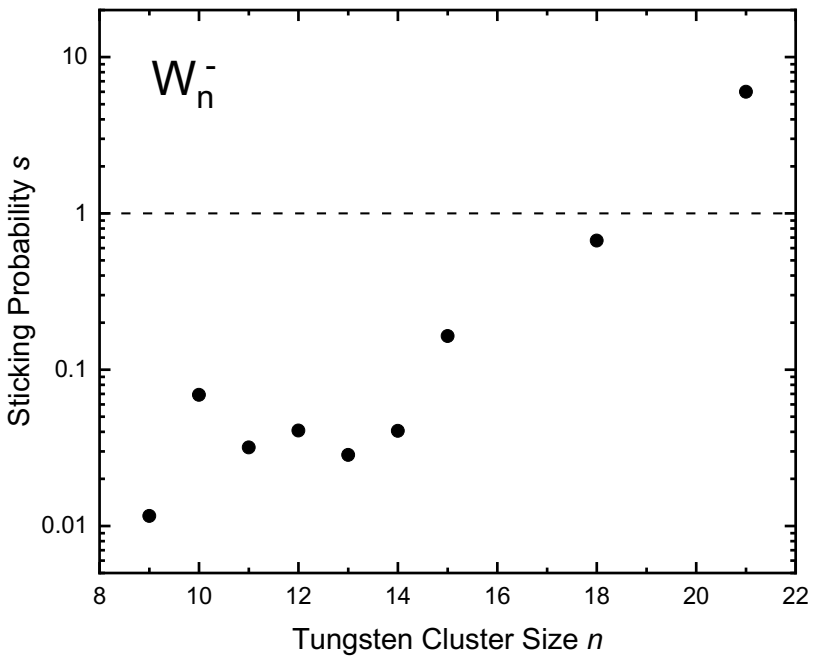

Figure 6: sticking probability s as a function of anionic tungsten cluster size n. Error bars are not represented and are about plus/minus a factor 10.

5. Thermionic emission from dianions: tunneling effects in the electron attachment

In the case of thermionic emission from doubly charged anions (dianions), the reverse process is the electron attachment to the singly charged anions. A model has been developed for comparison to the experimental KERD of the fullerene dianions C_{84}^{2-} and C_{90}^{2-}.[25,35] It includes only the capture step, and does not deal with IVR. The potential $V(r)$ felt by the electron is quite different from the case of the electron emission from the anions: it is repulsive in the long range and it is dominated by the Repulsive Coulomb Barrier (RCB) at short range. An approximate expression is proposed for the fullerene dianions in the frame of an electrostatic modeling:[25,35]

$$V(r) = \frac{e^2}{4\pi\varepsilon_0 r} - \frac{\alpha}{2(4\pi\varepsilon_0)^2 r^4}\left[1 + \frac{2\varepsilon_r + 4}{2\varepsilon_r + 3}\left(\frac{r_0}{r}\right)^2\right] \qquad (17)$$

In this approach, the fullerene anion is treated as a classical dielectric sphere of dielectric constant ε_r and radius r_0. α denotes the polarizability of the neutral. This simple modeling provides two major outcomes, namely the height of the RCB and the second electron affinity. Both values fall in good agreement with photoelectron spectroscopy data.[35]

Consequently, a simple and intuitive expression is introduced for the capture cross section, namely a hard-sphere type formula with a capture radius set to the distance R_C where $V(r)$ reaches its maximum ε_C. Below the repulsive barrier, this formula is weighted by the electron tunneling probability $P(\varepsilon)$. The attachment cross section may be written as[25,35]

$$\sigma(\varepsilon) = P(\varepsilon)\pi R_C^2 \qquad \text{for } \varepsilon < \varepsilon_C \qquad (18a)$$

$$\sigma(\varepsilon) = \pi R_C^2 \qquad \text{for } \varepsilon > \varepsilon_C \qquad (18b)$$

The tunneling probability $P(\varepsilon)$ has been numerically calculated using the Wentzel-Kramers-Brillouin (WKB) expression[55]

$$P(\varepsilon) = exp\left(-\frac{2}{\hbar}\int \sqrt{2m_e(V(r) - \varepsilon)}dr\right) \qquad (19)$$

Taking into account tunneling in the attachment cross section is required by the experiment as described below and is the originality of this detailed-balance model. Conversely, previous applications of the detailed balance to delayed emission from fullerene dianions were based on the assumption of an over-the-barrier detachment process.[56,57] Nevertheless, in addition to tunneling, one should consider the reflection over the barrier. Although this quantum effect is at the same fundamental level as tunneling, it is rarely included in the models.[58] We plan to add the above-barrier reflection in an improved version of our model.

The experimental KERD of delayed electron emission from the fullerene dianion C_{84}^{2-} is reported in Fig. 6. A RCB height ε_C of 1.4 eV has been measured by photoelectron spectroscopy in a magnetic bottle.[59]

It is specified by a dashed line in Fig. 7, marking the separation between the regime of tunneling detachment ($\varepsilon < \varepsilon_C$) and over-the-barrier detachment ($\varepsilon > \varepsilon_C$). Thus the experimental KERD demonstrates that most of the emitted electrons tunnel through the RCB.[25] Theoretical KERD is also reported in Fig. 6 and is parametrized by the daughter temperature ($T_d = 1175\ K$) calculated using the detailed balance decay rate (i.e., Eq. (5) integrated over ε ; see ref. [35] for more detail) and the experimental delay. Nice agreement is found between experiment and theory, especially since no adjustable parameter has been used for obtaining the theoretical distribution (except an intensity factor).

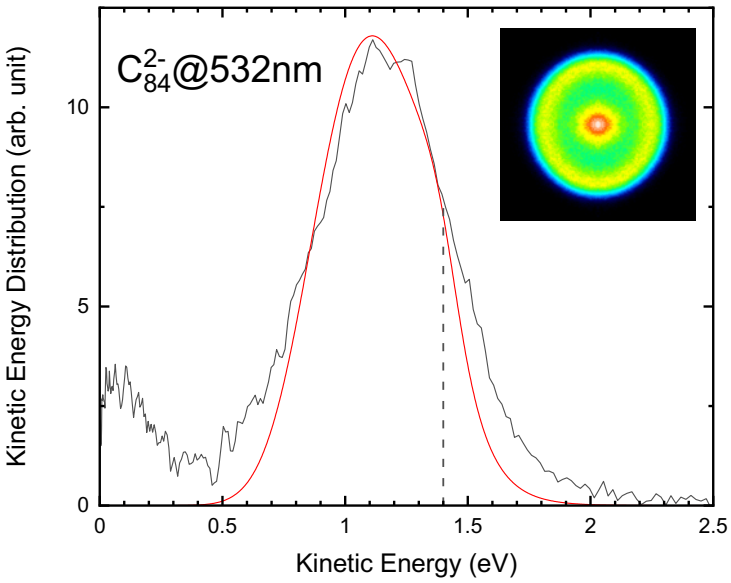

Figure 7: measured KERD (black) of thermionic emission from photoexcited C_{84}^{2-} dianions compared to the detailed balance calculation (red). The raw image is given in inset. The delay relatively to the 532 nm laser pulse is 150 ns. The low-energy feature (below 0.5 eV) results from the thermionic emission of singly charged anions C_{84}^{-} produced from the dianions C_{84}^{2-} after photon absorption. The dashed line indicates the RCB height and marks the limit between tunneling and over-the-barrier electron emission. The theoretical distribution is calculated without any adjustable parameter.

6. Conclusion and perspectives

Measurements of the KERD of thermionic emission in a VMI spectrometer using time resolution has been shown to be a powerful method to get insight into the reverse process, namely the electron attachment to the parent. Thermionic emission of a number of representative anions have been studied giving information on the electron attachment to the corresponding neutral system: small tungsten clusters, as a prototype of metal cluster, various fullerenes with different symmetries and the model molecule SF_6 with its unique properties in electron attachment (huge cross section only due to the electronic s-wave). It has been shown for all these systems that the classical Langevin model of electron capture is insufficient and the IVR must be included. An estimate for the IVR magnitude as a function of the electronic orbital angular momentum has been deduced from the KERD measurement.

Experimental KERDs of thermionic emission from fullerene dianions have provided information on the electron attachment to the corresponding fullerene anion. They have demonstrated that most of the electrons tunnel through the repulsive Coulomb barrier, at variance with previous studies.

All measurements have been done for a single delay: generally, about 100 ns (for photoinduced electron emission), and for SF_6^-, about 40 µs (for spontaneous electron emission). The next step would be to measure the KERD as a function of delay over a broad time range. It would allow a more stringent test of the detailed balance models, and, in particular, of the modeling of the electron attachment. Besides, it would allow to estimate the influence of radiative cooling on the electron emission as a function of the delay. It would give a full picture of the decay of these systems.

Measurement of electron KERD over a broad time range was performed earlier in our group in the case of photoexcited neutral C_{60}.[60] Such a measurement was possible on neutrals due to their reduced velocity, as compared to ions, allowing collection of the photoelectrons in the VMI interaction region up to delays as large as 10 µs. Extending the delay values over longer times for ions, with typical kinetic energies on the order of keV, would require building a specific device allowing ion trapping in a resonant cavity, in combination with the VMI geometry. In comparison to previously developed setups,[61,62] the challenge for our team would be to find a design allowing high electron count rate.

Acknowledgments

The long-term study presented in this review is the result of the work of many collaborators over time. In particular, we wish to acknowledge the contributions from B. Baguenard, M. Barbaire, M. Broyer, F. Calvo, C. Clavier, B. Climen, F. Lépine, M.A. Lebeault, S. Martin, G. Montagne, F. Pagliarulo, P. Parneix, J.C. Pinaré, and J.B. Wills.

We thank CNRS and “Agence Nationale de la Recherche” (ANR Dianes, ANR-06-BLAN-0041) for financial support.

References

(1) Campbell, E. E. B.; Levine, R. D. Delayed Ionization and Fragmentation En Route to Thermionic Emission: Statistics and Dynamics. *Annu. Rev. Phys. Chem.* **2000**, *51* (1), 65–98.

(2) Andersen, J. U.; Bonderup, E.; Hansen, K. Thermionic Emission from Clusters. *J. Phys. B At. Mol. Opt. Phys.* **2002**, *35* (5), R1.

(3) Hansen, K. *Statistical Physics of Nanoparticles in the Gas Phase*; Springer Series on Atomic, Optical, and Plasma Physics; Springer International Publishing: Cham, 2018; Vol. 73.

(4) Amrein, A.; Simpson, R.; Hackett, P. Multiphoton Excitation, Ionization, and Dissociation Decay Dynamics of Small Clusters of Niobium, Tantalum, and Tungsten: Time-resolved Thermionic Emission. *J. Chem. Phys.* **1991**, *95* (3), 1781–1800.

(5) Campbell, E. E. B.; Ulmer, G.; Hertel, I. V. Delayed Ionization of C_{60} and C_{70}. *Phys. Rev. Lett.* **1991**, *67* (15), 1986–1988.

(6) Wurz, P.; Lykke, K. R. Multiphoton Excitation, Dissociation, and Ionization of Fullerene (C_{60}). *J. Phys. Chem.* **1992**, *96* (25), 10129–10139.

(7) Hansen, K.; Echt, O. Thermionic Emission and Fragmentation of C_{60}. *Phys. Rev. Lett.* **1997**, *78* (12), 2337–2340.

(8) Andersen, J. U.; Brink, C.; Hvelplund, P.; Larsson, M. O.; Nielsen, B. B.; Shen, H. Radiative Cooling of C_{60}. *Phys. Rev. Lett.* **1996**, *77* (19), 3991–3994.

(9) Rajput, J.; Lammich, L.; Andersen, L. H. Measured Lifetime of SF_6^-. *Phys. Rev. Lett.* **2008**, *100* (15), 153001.

(10) Menk, S.; Das, S.; Blaum, K.; Froese, M. W.; Lange, M.; Mukherjee, M.; Repnow, R.; Schwalm, D.; von Hahn, R.; Wolf, A. Vibrational Autodetachment of Sulfur Hexafluoride Anions at Its Long-Lifetime Limit. *Phys. Rev. A* **2014**, *89* (2), 022502.

(11) Ito, G.; Furukawa, T.; Tanuma, H.; Matsumoto, J.; Shiromaru, H.; Majima, T.; Goto, M.; Azuma, T.; Hansen, K. Cooling Dynamics of Photoexcited C_6^- and C_6H^-. *Phys. Rev. Lett.* **2014**, *112* (18), 183001.

(12) Kono, N.; Suzuki, R.; Furukawa, T.; Matsumoto, J.; Tanuma, H.; Shiromaru, H.; Azuma, T.; Hansen, K. Electronic and Vibrational Radiative Cooling of the Small Carbon Clusters C_4^- and C_6^-. *Phys. Rev. A* **2018**, *98* (6), 063434.

(13) Bull, J. N.; Scholz, M. S.; Carrascosa, E.; Kristiansson, M. K.; Eklund, G.; Punnakayathil, N.; de Ruette, N.; Zettergren, H.; Schmidt, H. T.; Cederquist, H.; Stockett, M. H. Ultraslow Radiative Cooling of C_n^- (n = 3–5). *J. Chem. Phys.* **2019**, *151* (11), 114304.

(14) Stockett, M. H.; Bull, J. N.; Buntine, J. T.; Carrascosa, E.; Anderson, E. K.; Gatchell, M.; Kaminska, M.; Nascimento, R. F.; Cederquist, H.; Schmidt, H. T.; Zettergren, H. Radiative Cooling of Carbon Cluster Anions C_{2n+1}^- (n = 3–5). *Eur. Phys. J. D* **2020**, *74* (7), 150.

(15) Weidele, H.; Kreisle, D.; Recknagel, E.; Schulze Icking-Konert, G.; Handschuh, H.; Ganteför, G.; Eberhardt, W. Thermionic Emission from Small Clusters: Direct Observation of the Kinetic Energy Distribution of the Electrons. *Chem. Phys. Lett.* **1995**, *237* (5–6), 425–431.

(16) Chandler, D. W.; Houston, P. L. Two-dimensional Imaging of State-selected Photodissociation Products Detected by Multiphoton Ionization. *J. Chem. Phys.* **1987**, *87* (2), 1445–1447.

(17) Helm, H.; Bjerre, N.; Dyer, M. J.; Huestis, D. L.; Saeed, M. Images of Photoelectrons Formed in Intense Laser Fields. *Phys. Rev. Lett.* **1993**, *70* (21), 3221–3224.

(18) Eppink, A. T. J. B.; Parker, D. H. Velocity Map Imaging of Ions and Electrons Using Electrostatic Lenses: Application in Photoelectron and Photofragment Ion Imaging of Molecular Oxygen. *Rev. Sci. Instrum.* **1997**, *68* (9), 3477–3484.

(19) Pinaré, J. C.; Baguenard, B.; Bordas, C.; Broyer, M. Photoelectron Imaging Spectroscopy of Small Clusters: Evidence for Non-Boltzmannian Kinetic-Energy Distribution in Thermionic Emission. *Phys. Rev. Lett.* **1998**, *81* (11), 2225–2228.

(20) Baguenard, B.; Wills, J. B.; Pagliarulo, F.; Lépine, F.; Climen, B.; Barbaire, M.; Clavier, C.; Lebeault, M. A.; Bordas, C. Velocity-Map Imaging Electron Spectrometer with Time Resolution. *Rev. Sci. Instrum.* **2004**, *75* (2), 324–328.

(21) Wills, J. B.; Pagliarulo, F.; Baguenard, B.; Lépine, F.; Bordas, C. Time and Kinetic Energy Resolved Delayed Electron Emission in Small Carbon Cluster Anions. *Chem. Phys. Lett.* **2004**, *390* (1–3), 145–150.
(22) Calvo, F.; Lépine, F.; Baguenard, B.; Pagliarulo, F.; Concina, B.; Bordas, C.; Parneix, P. Evidence for Cluster Shape Effects on the Kinetic Energy Spectrum in Thermionic Emission. *J. Chem. Phys.* **2007**, *127* (20), 204312.
(23) Concina, B.; Baguenard, B.; Calvo, F.; Bordas, C. Kinetic Energy Spectra in Thermionic Emission from Small Tungsten Cluster Anions: Evidence for Nonclassical Electron Capture. *J. Chem. Phys.* **2010**, *132* (10), 104307.
(24) Concina, B.; Lépine, F.; Bordas, C. Thermionic Emission as a Probe of Low-Energy Electron Attachment to Fullerenes. *Phys. Rev. A* **2014**, *90* (3), 033415.
(25) Concina, B.; Lépine, F.; Bordas, C. Delayed Electron Emission from Fullerene Dianions: Evidence for a Thermal Tunneling Detachment. *Phys. Rev. A* **2015**, *92* (2), 023410.
(26) Concina, B.; Montagne, G.; Martin, S.; Bordas, C. Kinetic Energy Released in the Vibrational Autodetachment of Sulfur Hexafluoride Anion. *J. Chem. Phys.* **2021**, *154* (23), 234306.
(27) Weisskopf, V. Statistics and Nuclear Reactions. *Phys. Rev.* **1937**, *52* (4), 295–303.
(28) Elhamidi, O.; Pommier, J.; Abouaf, R. Low-Energy Electron Attachment to Fullerenes and in the Gas Phase. *J. Phys. B At. Mol. Opt. Phys.* **1997**, *30* (20), 4633–4642.
(29) Ptasińska, S.; Echt, O.; Denifl, S.; Stano, M.; Sulzer, P.; Zappa, F.; Stamatovic, A.; Scheier, P.; Märk, T. D. Electron Attachment to Higher Fullerenes and to $Sc_3N@C_{80}$. *J. Phys. Chem. A* **2006**, *110* (27), 8451–8456.
(30) Braun, M.; Marienfeld, S.; Ruf, M.-W.; Hotop, H. High-Resolution Electron Attachment to the Molecules CCl_4 and SF_6 over Extended Energy Ranges with the (EX)LPA Method. *J. Phys. B At. Mol. Opt. Phys.* **2009**, *42* (12), 125202.
(31) Vogt, E.; Wannier, G. H. Scattering of Ions by Polarization Forces. *Phys. Rev.* **1954**, *95* (5), 1190–1198.
(32) Hotop, H.; Ruf, M.-W.; Allan, M.; Fabrikant, I. I. Resonance and Threshold Phenomena in Low-Energy Electron Collisions with Molecules and Clusters. In *Advances In Atomic, Molecular, and Optical Physics*; Elsevier, 2003; Vol. 49, pp 85–216.
(33) Troe, J.; Miller, T. M.; Viggiano, A. A. On the Accuracy of Thermionic Electron Emission Models. I. Electron Detachment from SF_6^-. *J. Chem. Phys.* **2009**, *130* (24), 244303.
(34) Viggiano, A. A.; Friedman, J. F.; Shuman, N. S.; Miller, T. M.; Schaffer, L. C.; Troe, J. Experimental and Modeling Study of Thermal Rate Coefficients and Cross Sections for Electron Attachment to C_{60}. *J. Chem. Phys.* **2010**, *132* (19), 194307.
(35) Concina, B.; Lépine, F.; Bordas, C. A Detailed-Balance Model for Thermionic Emission from Polyanions: The Case of Fullerene Dianions. *J. Chem. Phys.* **2017**, *146* (22), 224311.
(36) Wang, X.-B.; Wang, L.-S. Observation of Negative Electron-Binding Energy in a Molecule. *Nature* **1999**, *400* (6741), 245–248.
(37) Xing, X.-P.; Wang, X.-B.; Wang, L.-S. Imaging Intramolecular Coulomb Repulsions in Multiply Charged Anions. *Phys. Rev. Lett.* **2008**, *101* (8), 083003.
(38) Wang, X.-B.; Wang, L.-S. Photoelectron Spectroscopy of Multiply Charged Anions. *Annu. Rev. Phys. Chem.* **2009**, *60* (1), 105–126.
(39) Concina, B.; Papalazarou, E.; Barbaire, M.; Clavier, C.; Maurelli, J.; Lépine, F.; Bordas, C. An Instrument Combining an Electrospray Ionization Source and a Velocity-Map Imaging Spectrometer for Studying Delayed Electron Emission of Polyanions. *Rev. Sci. Instrum.* **2016**, *87* (3), 033103.
(40) Martin, S.; Bernard, J.; Montagne, G.; Brédy, R.; Concina, B.; Chen, L. First Experiments Using a Table-Top Electrostatic Ion Storage Ring, the Mini-Ring. *J. Phys. Conf. Ser.* **2012**, *388* (10), 102011.
(41) Concina, B.; Lépine, F.; Martin, S.; Bordas, C. Coupling of a Velocity-Map Imaging Spectrometer with an Electron Cyclotron Resonance Ion Source. *J. Phys. Conf. Ser.* **2020**, *1412*, 242002.
(42) Hansen, K. Statistical Emission Processes of Clusters. *Philos. Mag. B* **1999**, *79* (9), 1413–1425.

(43) Hansen, K.; Campbell, E. E. B.; Echt, O. The Frequency Factor in Statistical Fullerene Decay. *Int. J. Mass Spectrom.* **2006**, *252* (2), 79–95.
(44) Andersen, J. U.; Bonderup, E.; Hansen, K. On the Concept of Temperature for a Small Isolated System. *J. Chem. Phys.* **2001**, *114* (15), 6518–6525.
(45) Lépine, F.; Bordas, C. Time-Dependent Spectrum of Thermionic Emission from Hot Clusters: Model and Example of C_{60}. *Phys. Rev. A* **2004**, *69* (5), 053201.
(46) Eisfeld, W. Highly Accurate Determination of the Electron Affinity of SF_6 and Analysis of Structure and Photodetachment Spectrum of SF_6^-. *J. Chem. Phys.* **2011**, *134* (5), 054303.
(47) Whitten, G. Z.; Rabinovitch, B. S. Accurate and Facile Approximation for Vibrational Energy-Level Sums. *J. Chem. Phys.* **1963**, *38* (10), 2466–2473.
(48) Andersen, J. U.; Gottrup, C.; Hansen, K.; Hvelplund, P.; Larsson, M. O. Radiative Cooling of Fullerene Anions in a Storage Ring. *Eur. Phys. J. D* **2001**, *17* (2), 189–204.
(49) Tomita, S.; Andersen, J. U.; Hansen, K.; Hvelplund, P. Stability of Buckminsterfullerene, C_{60}. *Chem. Phys. Lett.* **2003**, *382* (1–2), 120–125.
(50) Dashevskaya, E. I.; Maergoiz, A. I.; Troe, J.; Litvin, I.; Nikitin, E. E. Low-Temperature Behavior of Capture Rate Constants for Inverse Power Potentials. *J. Chem. Phys.* **2003**, *118* (16), 7313.
(51) Nikitin, E. E.; Troe, J. Electron Capture by Finite-Size Polarizable Molecules and Clusters. *Phys. Chem. Chem. Phys.* **2010**, *12* (31), 9011.
(52) Kikuchi, K.; Nakahara, N.; Wakabayashi, T.; Suzuki, S.; Shiromaru, H.; Miyake, Y.; Saito, K.; Ikemoto, I.; Kainosho, M.; Achiba, Y. NMR Characterization of Isomers of C_{78}, C_{82} and C_{84} Fullerenes. *Nature* **1992**, *357* (6374), 142–145.
(53) Troullier, N.; Martins, J. L. Structural and Electronic Properties of C_{60}. *Phys. Rev. B* **1992**, *46* (3), 1754–1765.
(54) Kasperovich, V.; Tikhonov, G.; Kresin, V. V. Low-Energy Electron Capture by Free C_{60} and the Importance of Polarization Interaction. *Chem. Phys. Lett.* **2001**, *337* (1–3), 55–60.
(55) Landau, L. D.; Lifshitz, E. M. *Quantum Mechanics: Non-Relativistic Theory.*; Elsevier Science: London, 2014.
(56) Compton, R. N.; Tuinman, A. A.; Klots, C. E.; Pederson, M. R.; Patton, D. C. Electron Attachment to a Negative Ion: $e + C_{84}^- \rightleftharpoons C_{84}^{2-}$. *Phys. Rev. Lett.* **1997**, *78* (23), 4367–4370.
(57) Concina, B.; Neumaier, M.; Hampe, O.; Kappes, M. M. Electron Emission from Laser-Heated Fullerene Dianions: Probing the Repulsive Coulomb Barrier. *J. Chem. Phys.* **2008**, *128* (13), 134306.
(58) Hansen, K. Tunneling and Reflection in Unimolecular Reaction Kinetic Energy Release Distributions. *Chem. Phys. Lett.* **2018**, *693*, 66–71.
(59) Wang, X.-B.; Woo, H.-K.; Yang, J.; Kappes, M. M.; Wang, L.-S. Photoelectron Spectroscopy of Singly and Doubly Charged Higher Fullerenes at Low Temperatures: C_{76}^-, C_{78}^-, C_{84}^- and C_{76}^{2-}, C_{78}^{2-}, C_{84}^{2-}. *J. Phys. Chem. C* **2007**, *111* (48), 17684–17689.
(60) Lépine, F.; Climen, B.; Lebeault, M. A.; Bordas, C. Time-Dependent Delayed Electron Spectra: A Direct Measurement of Total Decay Rate as a Function of Internal Energy. *Eur. Phys. J. D* **2009**, *55* (3), 627–635.
(61) Johnson, C. J.; Shen, B. B.; Poad, B. L. J.; Continetti, R. E. Photoelectron-Photofragment Coincidence Spectroscopy in a Cryogenically Cooled Linear Electrostatic Ion Beam Trap. *Rev. Sci. Instrum.* **2011**, *82* (10), 105105.
(62) Saha, K.; Prabhakaran, A.; Chandrasekaran, V.; Rappaport, M. L.; Heber, O.; Zajfman, D. An Experimental Setup to Study Delayed Electron Emission upon Photoexcitation of Trapped Polyatomic Anions. *Rev. Sci. Instrum.* **2017**, *88* (5), 053101.